Silicon Photonic Ring-Assisted Mach-Zehnder Modulators: Theory, Design, and Performance

Mustafa Hammood

Department of Electrical and Computer Engineering, University of British Columbia, 2332 Main Mall, Vancouver, BC, V6T1Z4, Canada

ABSTRACT

Modulators are a key building block to any optical communication link. Realizing high-performance silicon photonic modulators is key to the success of this technology. In this work we discuss silicon photonic ring-assisted Mach-Zehnder interferometer (RAMZI)-based modulators and their theory, design, and operation principles. We present the operation principle when using these modulators for On-Off Keying (OOK) and Quadrature Amplitude Modulation (QAM) formats. We present the simulation results of such a modulator when used for OOK modulation of speeds up-to 50 Gbps and show their superior performance to similar micro-ring resonated-based modulators. Additionally, we show how I-Q modulation is performed using RAMZI modulators. Traditionally I-Q modulation is done using Mach-Zehnder modulations, due to the fact that micro-ring modulators module both, the amplitude and phase simultaneously. A RAMZI modulator is unique because it allows for in-phase and quadrature modulation while using a footprint similar to that of a micro-ring resonator. We present the simulation results of a RAMZI modulator used in a QPSK coherent transmission link operating at 12.5 Gbaud.

Keywords: Silicon-on-insulator, Silicon photonics, Micro-ring resonator, Mach-Zehnder Interferometer, Modulator

1. INTRODUCTION

Silicon integrated circuits created the modern micro-electronics industry. We are reaching a turning point in which data bandwidth requirements cannot be met by traditional copper electrical interconnects. Optical communications must be employed to accommodate such increased bandwidths and break the interconnects bottlenecks. Silicon photonics is a technology that can achieve on-chip optical communication at the micron-scale. Silicon photonics uses many of the advances in the micro-electronics industry to realize photonic integrated circuits using similar fabrication platforms and processes.[1]

In optical communications, modulators are the workhorse of the communication network. Modulators can appear at the transmitter side of an optical link and are the components that encode the data onto a carrier optical signal. Realizing high-performance optical communication links using silicon photonics technology will require high-performance modulators.[2] Some of the performance figures-of-merit (FOMs) of an optical modulator include the modulator's bandwidth, linearity, drive voltage, insertion loss, and extinction ratio. Silicon photonic modulators must also consider the sensitivity to fabrication variations and device on-chip footprint. Future optical communication links require compact and energy-efficient modulators.

An optical modulator applies a phase-shift to an optical signal, this phase-shift is utilized to modulate the intensity and phase of the signal by the use of interferometric or resonant structures. Such a phase-shift can be made using various methods, carrier depletion in reverse-bias lateral PN diodes is a popular method in which the modification of the free-carrier concentrations inside the waveguide results in a modification of the materials refractive index via the plasma-dispersion effect.[3] better, high-efficiency approaches such as using silicon-insulator-silicon capacitors (SISCAPs)[4,5] and PIPIN junctions[6] have been demonstrated, however using such approaches increases the process complexity and reduces the fabrication tolerances.

Send correspondence to Mustafa Hammood.
E-mail: mustafa@ece.ubc.ca

1.1 Modulators in Silicon Photonics Technologies

There are several devices in which the phase-shift can be utilized to modulate an optical signal. The various devices can be classified into two sub-categories: 1) interferometric-based devices such as Mach-Zehnder (MZ) interferometer modulators and Michelson interferometer modulators, and 2) resonance-based devices such micro-ring resonator (MRR) modulators and slow-light effect modulators.[7]

1.1.1 Mach-Zehnder Modulators

MZ modulators, shown in Fig. 1, apply the phase shift to the arms of an MZ interferomter. By increasing the phase difference between the two arms, the two beams of light destructively interfere when recombined at the output of the interferometer. Silicon photonic MZ modulators are useful for data communication applications due to their high thermal insensitivity and wide optical bandwidth.[8]

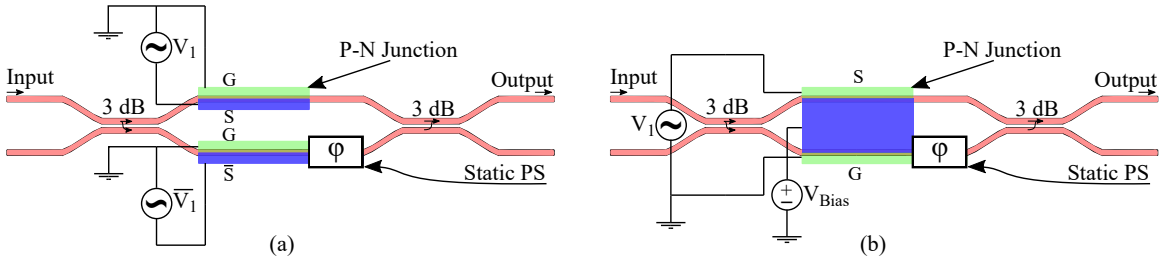

Figure 1. A schematic of Mach-Zehnder modulators made using 3 dB directional couplers operated in a (a) Dual-drive parallel push-pull and (b) Single-drive series push-pull scheme.

MZ modulators are typically operated in a push-pull (PP) dual-drive (DD) configuration, namely, the two phase-shifters on each arm are actuated with opposite signals according to the data-stream.[9] Such an operation scheme ensures that the modulator has little frequency chirp and can be driven by low-voltage swings. The low voltage swing operation is a critical requirement if CMOS drivers were to be used to control the modulator. Other driving schemes include single-drive (SD), series-push-pull (SPP),[10] shown in Fig. X(b). Such scheme increases the electro-optical bandwidth of the modulator and simplifies the driver configuration, since it uses a single RF source instead of two.[10] However, using this scheme increases the voltage swing required to achieve the same amount of phase shift when compared to a DD-PP configuration.[11]

The phase-shifting sections in an MZ modulator can be made using a lumped-element configuration or a travelling-wave configuration. A lumped-element configuration refers to a phase-shifting section that is relatively short compared to the RF wavelength of the electrical, driving signal. Such a configuration can be considered a point load from the electrical perspective. A typical criterion for the phase-shifter length is that it has to be below 1/10th of the free-space RF wavelength, λ_{RF}, divided by the RF effective index n_{RF}.[9] Using travelling-wave electrodes can yield much higher electro-optical bandwidths than their lumped-element counterpart. However, this increase in bandwidth comes at the expense of higher energy consumption and greater design complexity of due to the optimization required to ensure that the impedance of the source, electrodes, and termination are matched, and that the RF phase velocity matches that of the optical group velocity.[12,13] Using either electrode configurations dictates a trade-off between the electro-optical bandwidth, drive voltage, and energy per bit consumption. While travelling-wave electrodes are generally much longer in length compared to lumped-element electrodes, both configurations have a generally very large footprint compared to MRR modulators.

The MZ interferometer can be made by using either 1-by-2 3 dB power splitters (Y-splitters) or 2-by-2 3 dB power splitters (directional couplers). The advantage of using Y-splitters is that the extinction ratio of the interferometer can be made to be extremely large, as the Y-splitters have very little power splitting imbalance as compared to typical directional couplers.[14] Additionally, using Y-splitters allows for a much wider operation wavelength range, as Y-splitters are typically wider in bandwidth compared to typical directional couplers.[15] The advantage of using directional couplers is that the second output port allows to easily monitor any the phase imbalance between the arms of the interferometer, which is needed when biasing the modulator around

the quadrature point ($\pi/2$) of the MZ interferometer. Note that the $\pi/2$ quadrature biasing point here is only required for On-Off Keying (OOK) operation, the modulate needs to be biased around the zero-transmission point (π) when used in Quadrature-Amplitude Modulaiton (QAM). Further discussion on the various modulation formats on section 1.2.

1.1.2 Micro-Ring Resonator Modulators

CMOS-compatible silicon MRR modulators (shown in Fig. 2) have been demonstrated and keep attracting considerable research interest.[16–19] MRR modulators have been shown to reach high modulation speeds and occupy a very small footprint while achieving very high power per bit efficiency,[18] as low as 4.5 fj/bit.[20] However, these modulators suffer from limited optical bandwidth and strict wavelength dependence and therefore, need precise control over the resonant condition. In particular, modulation is usually achieved by shifting the MRR's intensity response, which constrains the MRR to be operated close to the critical coupling point to achieve a high extinction ratio,[16] hence making the device very sensitive to fabrication deviations.[21] Additionally, MRR modulators are restricted by their challenges for phase modulation and advanced modulation formats, low extinction ratio, large frequency chirp, wavelength stability due to thermal and process variations, and trade-offs between bandwidth and modulation efficiency. MRRs are not typically suitable for I-Q modulation formats as the modulation is bias-dependent because both, phase and intensity are modulated simultaneously with the applied signals.[22]

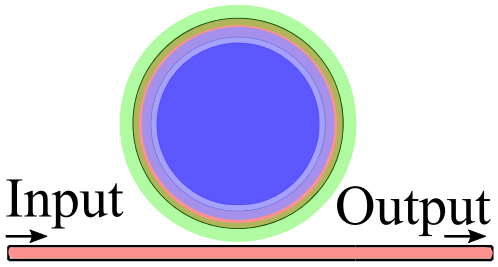

Figure 2. Schematic of how a P-N junction can be integrated inside the cavity of an all-pass micro-ring resonator to create an optical modulator. A second, drop-port can be introduced to actively monitor the resonant wavelength of the modulator and ensure it aligns with the operating point.

While MRR modulators have very low energy per bit relative to MZ modulators, the energy needed to tune and to lock the MRR's resonant wavelengths around the operation wavelength is very significant and would negate the advantage of lower power consumption gained.[8] Recent advances in active monitoring and stabilization of MRRs promises to enable the practical deployment of such devices in future systems.[23,24]

1.1.3 Micro-Ring-Assisted Mach-Zehnder Interferometer Modulators

As an alternative to using the MRR directly for intensity modulation, the steep phase response of an MRR can be used to achieve phase modulation, which can then be converted into intensity modulation by means of an MZ interferometer.[25,26] This is done in the Ring-assisted Mach-Zehnder interferometer (RAMZI) modulator configuration, shown in Fig. 3. In such a configuration, two MRRs (or more[27,28]) are loaded onto the two arms of the MZ interferometer in which the phase-response of the MRRs are used in place of the long waveguide phase-shifters.

Such a configuration can achieve both, the high extinction ratios that are characteristic of MZ modulators and the low drive voltages that are characteristic of MRR modulators. Additionally, MRRs in RAMZI must ideally be over-coulpled to have a 2π phase-shift across the resonance condition. Therefore, Using RAMZI modulators significantly increases the fabrication tolerance of the modulators as compared to MRR modulators, which need to be operated in the critical coupling regime.[21] In addition to the increased fabrication tolerance, due to their low Q, over-coupled MRRs have wider usable optical bandwidth as compared to their critically-coupled counterparts.[27]

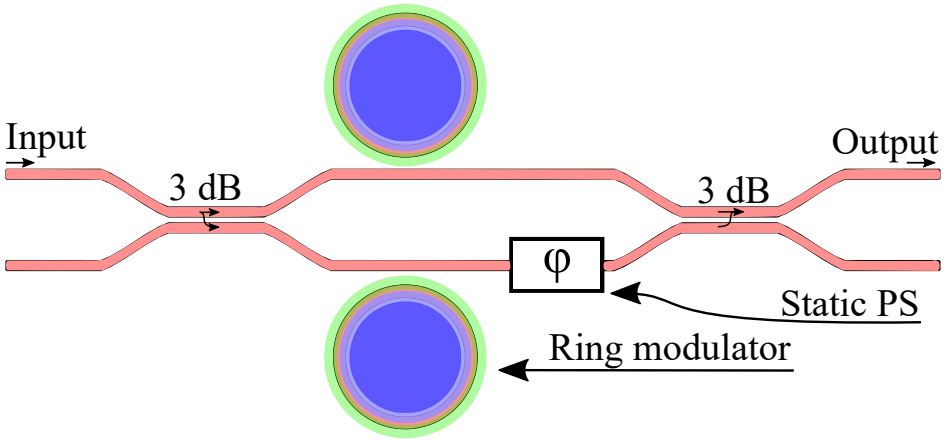

Figure 3. A schematic of a ring-assisted Mach-Zehnder Interferometer modulator made using two 3 dB directional couplers.

Another major advantage of the RAMZI configuration is that it has the potential to significantly reduce the temperature sensitivity of the MRR modulators. By carefully engineering the optical path lengths of each arm, one can design a passive, athermal MRR modulator that can operate over an extended temperature range.[29]

In this work, we will discuss and explain the operation principle of RAMZI modulators, compare their performance to typical MRR and MZ modulators, demonstrate various modulation formats realized using RAMZI modulators, and finally demonstrate a high-speed optical link made using RAMZI modulators that can operate at a transmission speed up-to 50 Gbit/s.

1.2 Modulation Formats

This subsection will briefly discuss and introduce the modulation formats used in our devices, namely, pulse-amplitude modulation (PAM) formats and in phase-quadrature (IQ) modulation formats.

1.2.1 Amplitude Modulation

On-Off-Keying (OOK) or PAM-2 can be described as a simple form of amplitude modulation where digital data (0 and 1) are presented in the form of absence or presence of light. OOK has been the main modulation format employed in short reach optical interconnects. The simplicity of the transmitter and receiver architectures have been an important factor in the success of OOK for short reach optical links. Recently deployed, 100 Gbps systems utilize OOK modulation in 4λ x 25 Gbps configuration. However, as we move towards 400 Gbps and 1 Tbps systems, OOK requires a proportional increase in the bandwidth. Hence, more efficient modulation formats are required to avoid such complexity. Two opposing approaches are being taken to scale up PAM formats to beyond 100 Gbps, the first being by increasing the number of wavelengths, as in the case of the CWDM8 MSA,[30] and the second is by employing higher-order modulation formats, e.g. PAM-4 and PAM-8, as in the case of the openEye MSA.[31] PAM-4 is another form of amplitude modulation where the 4 levels of amplitude are used to present data. The recent 200 Gbps and 400 Gbs IEEE Ethernet standard have been released,[32] and the PAM-4 modulation format has been selected for 400 Gbps systems using 4 lanes of 100 Gbps configuration.

PAM modulation provides a good balance between capacity and design complexity. Minimal modifications are required to the ROSA architecture when scaling up beyond PAM-2, since the intensity-modulation direct-detection (IM/DD) principle remains relatively similar.[33,34]

1.2.2 I-Q Modulation

Moving beyond 400 Gbps for short-reach interconnects is an open-ended question that poses a significant challenge to traditional PAM formats. To cope with such increases in data rate, other dimensions must be exploited such as polarization and complex modulation. I-Q modulation utilizes the phase domain in addition to the amplitude

domain to achieve higher interconnect bandwidths. Coherent transmission systems have been predominantly used for long haul communication systems.[34] The compact footprint and low fabrication cost of silicon photonic I-Q TOSAs, are two compelling arguments for exploring coherent systems on silicon photonic platforms. However, without a clear roadmap for what's beyond 400 Gbps, coherent transmission systems are poised to be a likely solution for such short-reach interconnects.[5,35]

While I-Q modulation formats have the potential of achieving higher data-rates while maintaining a simple TOSA architecture, the complexity of the ROSA architecture is significantly increased due to the need of local oscillators, advanced digital-signal-processing, and optical hybrids for coherent receiving systems.[33,34]

2. THEORY

To model the overall transfer function of the RAMZI device, we choose to apply the transfer-matrix method (TMM), as illustrated in Fig. 4. The total transfer function of the device is therefore given by:

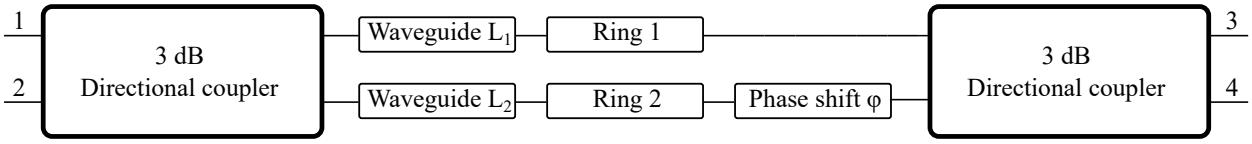

Figure 4. Representation of the transfer-matrix method model of the Ring-assisted Mach-Zehnder Interferometer.

$$M_{TOT} = M_{3dB} M_{WG} M_{Rings} M_{3dB} \tag{1}$$

Where M_{3dB}, M_{WG}, and M_{Rings} are the matrix representation for the 3 dB couplers, waveguides, and MRRs, respectively. These matrices are given by:

$$M_{3dB} = \begin{bmatrix} \frac{1}{\sqrt{2}} & \frac{-j}{\sqrt{2}} \\ \frac{-j}{\sqrt{2}} & \frac{1}{\sqrt{2}} \end{bmatrix} \; ; \; M_{WG} = \begin{bmatrix} 0 & \phi_{WG_1} \\ \phi_{WG_2} + \phi & 0 \end{bmatrix} \; ; \; M_{Rings} = \begin{bmatrix} 0 & T_{Ring1} \\ T_{Ring2} & 0 \end{bmatrix} \tag{2}$$

The transfer function of a given waveguides with length L_i is given by: $\phi_{WG_i} = exp(-j\beta_i L_i - \alpha L_i)$. Where α is the loss in dB/cm and $\beta_i = \frac{2\pi n_{eff}}{\lambda}$ is the propagation constant. The transfer function of the individual MRRs (Ring 1 and Ring 2 with radius R in Fig. 4) through-ports are given by:[36]

$$T_{ring} = \frac{t_1 - t_2\chi}{1 - t_1 t_2 \chi'} \; ; \; \chi = exp(-\alpha L_{ring} - j\beta L_{ring}) \; ; \; L_{ring} = 2\pi R \tag{3}$$

Using the combined matrix in Eq. 1, we can obtain an analytical representation of the RAMZI device.

2.1 Operation

In this section, using the analytical equations derived above, we will discuss how we choose to operate the RAMZI as a modulator. We will discuss the biasing scheme used for the MZ and the rings to achieve the highest possible extinction ratios and lowest possible insertion loss with the least possible driving voltage required. We will demonstrate how the RAMZI modulator is driven using push-pull operation. This driving scheme can be realized using either series single-drive or parallel dual-drive architectures, as previousily shown in Fig. 1.

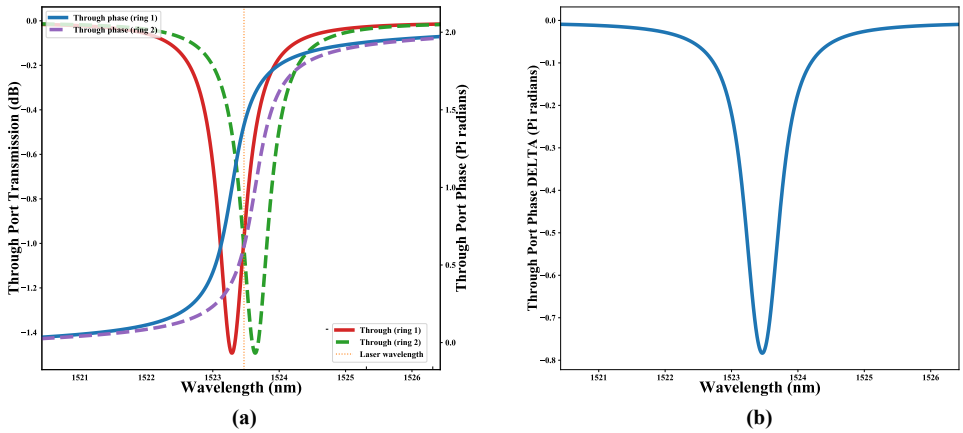

Figure 5. The biasing scheme of the two rings in the ring-assisted Mach-Zehnder interferometer as shown in (a) the phase and amplitude spectra and (b) the phase difference between the two arms.

2.1.1 Pulse-Amplitude Modulation

For OOK operation, the MZ operating point is set to negative slope quadrature point (i.e. $\pi/2$ difference between the two arms), such that the MZ transfer function slope is maximally linear.[37]

The push-pull driving scheme of the two MRRs is shown in Fig. 6. The two MRRs are then biased to be 0.78π apart in phase, as shown in Fig. 5. Such that when the MRRs are 'pulled' together due to electrical drive, the phase difference is reduced to $\pi/2$, which when added to the bias, initial $\pi/2$ difference between the arms, results in an overall π phase difference between the arms, resulting in a complete destructive interference and minimal transmission for the 'Off' state. Similarly, when the MRRs are 'pulled' apart due to electrical drive, the phase difference is increased, which is added to the bias, initial $\pi/2$ phase difference between arms, resulting in an overall phase difference of $\frac{3}{2}\pi$ in the 'On' state. The resultant output spectra of the RAMZI in the two states is shown in Fig. 7. This particular driving scheme will yield the highest possible extinction ratio with the least possible required drive voltage swing. The MRRs wavelength detuning bias depends on the quality factor of the ring modulator and the drive voltage swing. Other driving schemes can be explored in the supplemental Jupyter notebook to minimize insertion-loss at the expense of higher drive voltage swings.

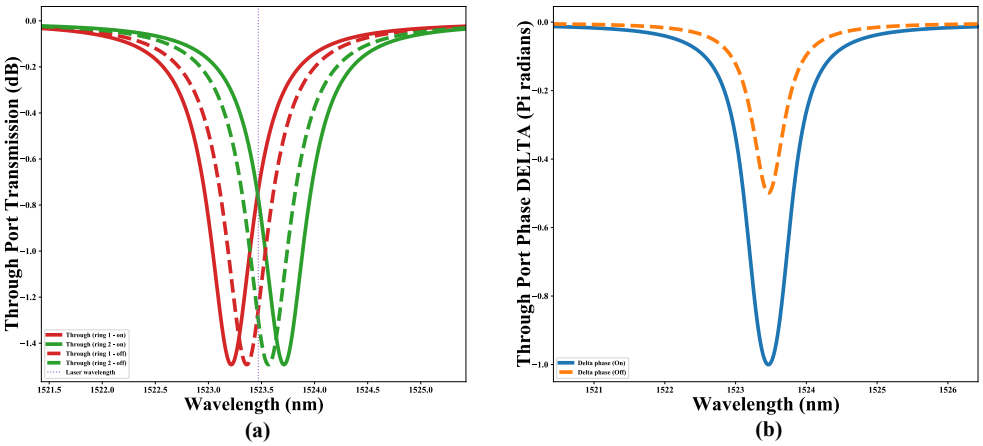

Figure 6. The operation scheme of the ring-assisted Mach-Zehnder modulator in On-Off Keying operation as shown in (a) the amplitude spectra of each arm in each of the two states and (b) the phase difference between the two arms in each of the two states.

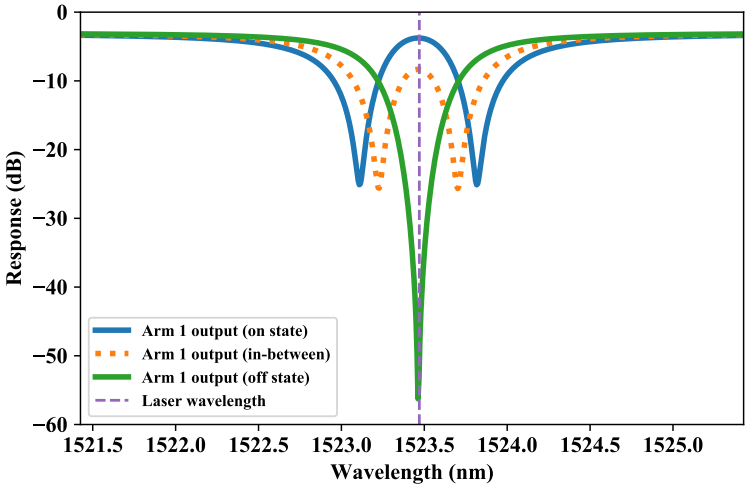

Figure 7. The operation scheme of the ring-assisted Mach-Zehnder modulator in On-Off Keying operation. The output spectrum of the two states is shown.

Such a driving scheme will result in an insertion loss of -3.11 dB and a maximal DC extinction ratio of $>$ 55 dB, with a voltage swing of only 0.8 V_{pp} using a simple lateral P-N diode design. Further discussion on the P-N diode phase-shifter design in section 3.1.

Another driving scheme where the insertion loss is minimized at the cost of increased drive voltage swing is by settings the rings 1.3π apart in phase. By increasing the drive voltage swing to 3.8 V_{pp}, when the rings are 'pushed' together, the effective total phase difference between the two arms is π, resulting in destructive interference. When the rings are 'pulled' apart, the effective total phase difference between the two arms is 1.85π, resulting in constructive interference. Such a driving scheme will result in an insertion loss of -0.57 dB and an extinction ratio of 24.5 dB.

2.1.2 I-Q Modulation

In the case of I-Q modulation, the resonances of the two MRRS are initially aligned with the input laser's wavelength. The MZ is biased at the zero-transmission point (π). The push-push operation causes the wavelength resonance of each MRR to 'swing' around the laser source's wavelength. Such an operation causes a change in-phase for the two states, resulting in a π phase difference between the two states, while the amplitude remains unchanged. This is shown in Fig. 8. This is effectively Binary Phase-Shift-Keying operation. This can be combined with a second amplitude modulation arm to effectively create an I-Q modulator for Quadrature Amplitude Modulation (QAM) formats, as shown in Fig. 9.

This configuration can be scaled up to multiple advanced I-Q modulation formats (QPSK, 16QAM, 64QAM) while maintaining the relatively small footprint of MRR modulators.

3. DESIGN AND SIMULATION

This section will detail and describe the design choices for the modulator and its sub-components, such as the rings and their P-N diodes, the thermo-optic heaters, and the 3 dB splitters/combiners. The overall CAD layout of the device is shown in Fig. 10. The total footprint was measured to be 90 x 190 μm^2 without electrical interconnects (see Fig. 10(a)) and 520 x 670 μm^2 with electrical interconnects and the RAMZI's monitoring circuit (see Fig. 10(b)).

The rings were designed to have a radius of 25 μm, 75% of which was covered with a P-N diode, a heater was placed on top of each to allow the tuning and biasing of the rings. The ring had a bus-to-ring gap of 150 nm, resulting in a power coupling coefficient of 0.35. Such a coupling coefficients allows the ring to operate in

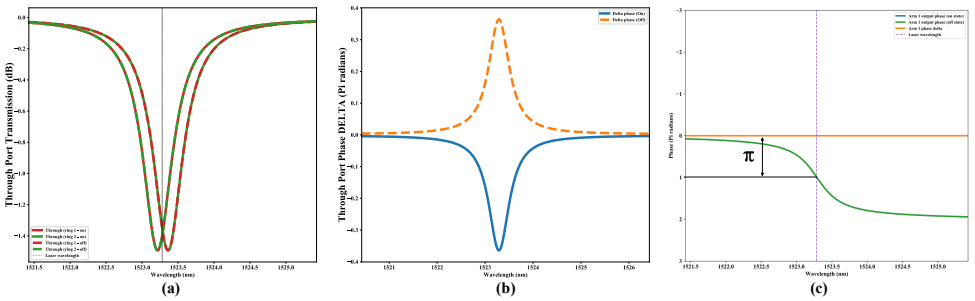

Figure 8. (a) Resonances of the two micro-rings in the ring-assisted Mach-Zehnder modulator in the two modulation states. (b) Phase-difference between the two arms of the modulator in the two modulation states. A π is observed. (c) Phase-response of the ring-assisted Mach-Zehnder modulator in the two states. The amplitude response remains the same, however, the phase is delayed by a π.

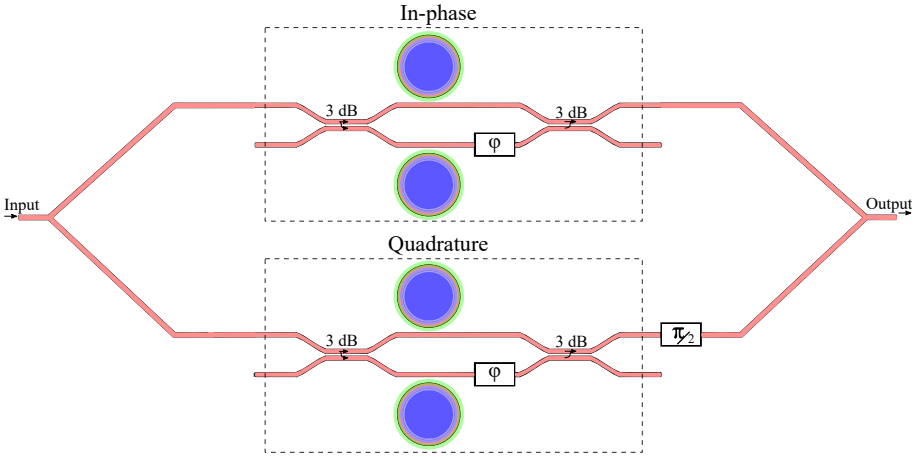

Figure 9. A schematic of a ring-assisted Mach-Zehnder Interferometer modulator when used in Quadrature Amplitude Modulation.

the over-coupling regime, minimizing the effects of fabrication variations and relaxes the requirement of being in the critical coupling regime. The ring-to-monitor gap was chosen to be 450 nm, the power coupled to the photodiode (PD) allows the tuning and monitoring of the resonant wavelength of the ring.

A 60 μm resistive heater was placed on top of the lower arm of the MZ interferometer to act as a thermo-optic phase-shifter to control the operating point of the MZ. Further efficient thermo-optic phase shifters designs can be explored using the same fabrication process.[38]

3.1 P-N Diode Design

There is a fundamental trade-off in the design of the P-N diode junction between bandwidth, modulation efficiency, V_π, optical loss,[39] and fabrication process complexity. The design of our P-N junction is shown in Fig. 11(a). We chose a simple lateral P-N junction made using 6 doping concentrations to minimize resistance and increase the bandwidth. The P++, P+, P, N, N+, and N++ implants had peak doping densities of 1e19/cm^3, 2e18/cm^3, 7e17/cm^3, 5e17/cm^3, 3e18/cm^3, and 1e19/cm^3, respectively. The P-N junction performance was simulated using Lumerical CHARGE, with the resulting C-V and I-V curves shown in Fig. 11(b).

The efficiency of a carrier depletion phase-shifter is highly dependent on the resultant depletion region that comes about from the applied voltage. The width of the depletion region as a function of the doping concentrations (N and P) and applied voltage (V) is given by:[3,40]

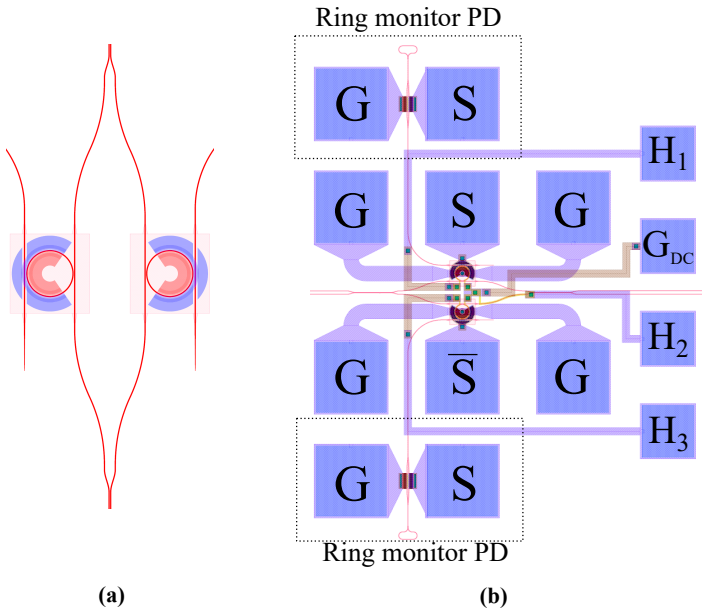

Figure 10. CAD mask-layout of the ring-assisted Mach-Zehnder modulator showing (a) the basic building blocks (directional couplers and rings) and (b) with all the electrical interconnects and drivers connected.

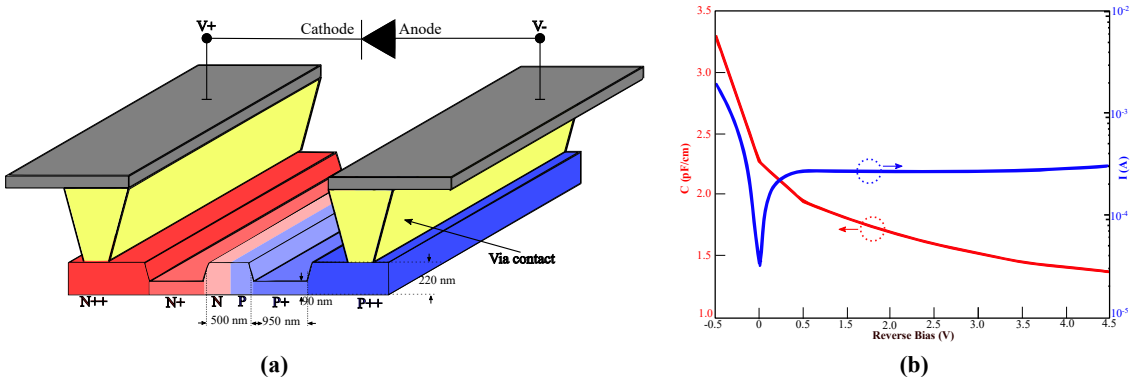

Figure 11. (a) Perspective view showing the design parameters of the lateral P-N junction and the electrical equivalent of the junction. (b) Simulated C-V and I-V curves of the lateral P-N junction used.

$$W(N,P,V) = \sqrt{\frac{2\epsilon_r\epsilon_o}{q}\frac{(V_{bi}-V)(N+P)}{NP}} \tag{4}$$

Where ϵ_r and ϵ_o are the relative permittivities of silicon and free-space, respectively. q is the fundamental electron charge 1.6e-19 C and V_{bi} is the built-in voltage potential given by:[3]

$$V_{bi} = \frac{kT}{q}\log(\frac{NP}{n_i^2}) \tag{5}$$

Where k is the Boltzmann constant 1.38e-23 j/K, n_i is the intrinsic carrier concentration 1.5e16 $/m^3$, and T is the temperature of the diode in Kelvins. Based on equations 4 and 5, we can estimate the width of the depletion region of our P-N diode device as shown in Fig. 12. Based on our CHARGE simulations, the resulting tuning efficiency of such a P-N diode is 25 pm/V when used in our designed MRRs configuration.

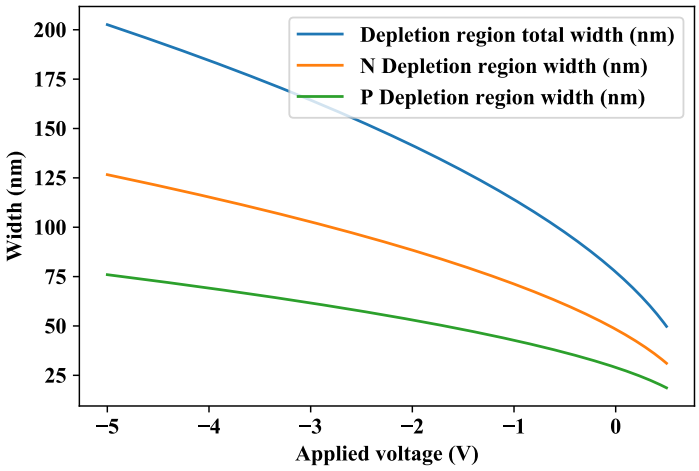

Figure 12. The calculated theoretical width of the depletion region based on the applied voltage and the fabrication process' doping parameters.

3.2 Simulation

In this section, using Lumerical INTERCONNECT, we simulate the operation of our RAMZI modulator and the designed P-N junction. We bias the rings and the arms of the interferometer according to the description in section 2.1. An ideal PRBS signal (2^{15}-1) is passed through a jitter element with a random jitter of 6% at the output of each NRZ generator. We simulate out RAMZI modulator using a drive voltage of only 0.5 V_{pp}. The output of the modulator is then received by a photodiode with a responsivity of 1.09 A/W, which is then passed through a Bessel low-pass filter with a bandwidth of 0.7 times the bit-rate. The resulting eye diagrams of a 5 km optical link are shown in Fig. 13(a) in various transmission speeds. To compare the perform ace of the RAMZI modulator to a typical MRR modulator, we used an MRR modulator in the same link instead. However, the drive voltage swing was increased to 1.5 V_{pp} for the eye to be sufficiently opened. The results are compared in Fig. 13(b).

The difference in quality of the transmission link between the two transmitters can be clearly seen. The simple MRR modulator has a significant overshoot at the rising edges which can be clearly seen from 2.5 Gbps to 25 Gbps. The MRR overshoot is characteristic feature of MRR modulators that occurs when the rise time of the modulator approaches the lifetime of the optical cavity.[41] While undesirable, this overshoot can be compensated for using a limited bandwidth photodiode and subsquent trans-impedance amplifiers.[42] The eye diagram of the RAMZI show a high linearity with no overshoot, as the overshoot response is cancelled out. Additionally, unlike the MRR modulator, the RAMZI modulator can reach almost zero optical power when transmitting in the 'Off' state due to the complete destructive interference, similar to the operation principle of MZ modulators.

3.2.1 I-Q Modulation

Similarly, we can apply the biasing scheme and configuration described in section 2.1.2 to operate the RAMZI modulator in QPSK modulation formats. The simulated coherent transmitter-receiver architecture is shown in Fig. 14.

The simulated constellation diagram is shown in Fig. 15 for a transmission rate of 12.5 Gbaud. The four symbols are clearly distinguishable at this data rate.

4. CONCLUSION

In conclusion, we have demonstrated and discussed the operation principle of a RAMZI modulator. We discussed how such modulators can be designed in a typical silicon photonics foundry process. We discussed and simulated

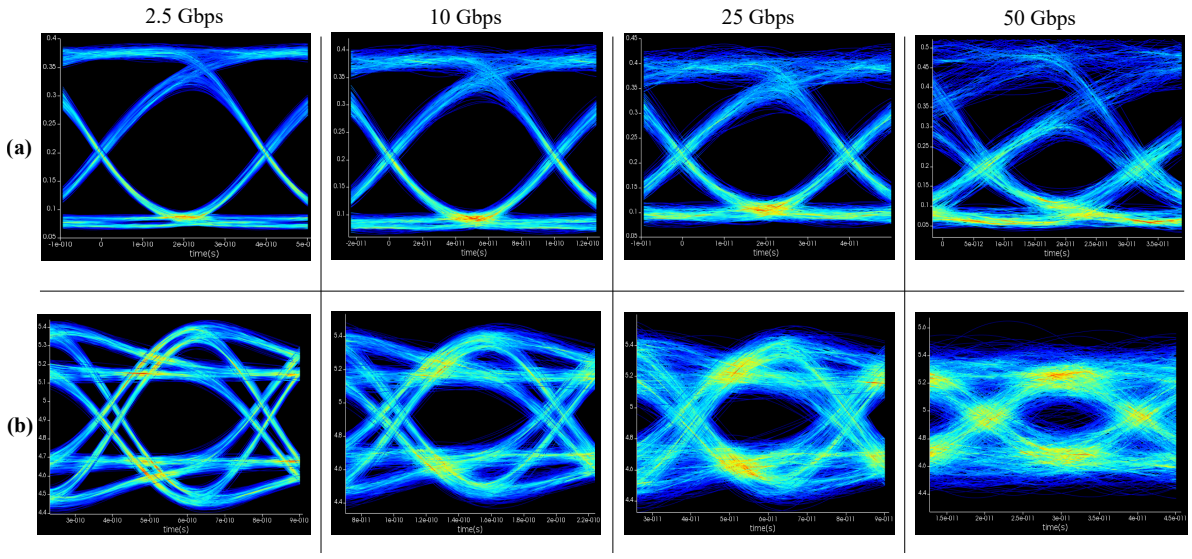

Figure 13. Simulated 2.5 Gpbs to 50 Gbps eye diagrams comparing (a) A ring-assisted Mach-Zehnder modulator driven by 0.5 V peak-to-peak and (b) A typical micro-ring modulator driven by 1.5 V peak-to-peak.

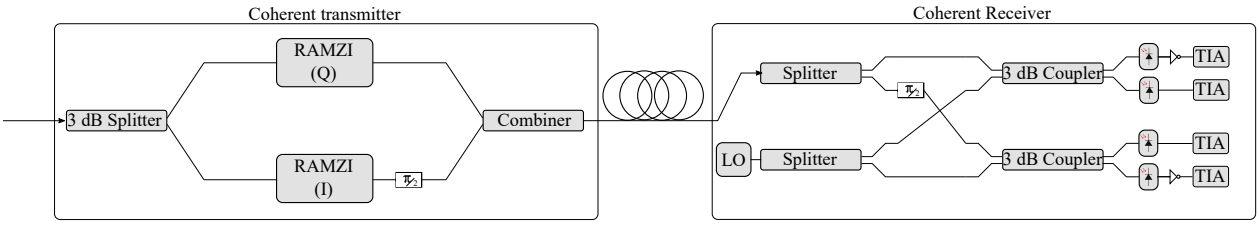

Figure 14. Schematic of the coherent transmitter-receiver link used in the simulation. The Local Oscillator (LO) is assumed to be perfectly in-phase with the input laser source.

how a RAMZI modulator can be used for OOK modulation up-to 50 Gbps with an extinction ratio of 5.7 dB. We additionally showed how a RAMZI modulator can be used for QAM formats such as the case of QPSK modulation of speeds up to 12.5 Gbaud. Such modulators have similar footprints to typical MRR modulators and can have higher performance metrics as regards their insertion loss, extinction ratio, modulation efficiency, and linearity.

Further work can be done to demonstrate how temperature phase-shift compensation techniques[29] can be applied to such modulators to enhance the operation temperature range and reduce the sensitivity to environmental variables.

4.1 Acknowledgments

We'd like to acknowledge Ajay Mistry for his input and insightful discussions and Lumerical for their support and assistance in troubleshooting the simulations.

REFERENCES

[1] Kimerling, L., Ahn, D., Apsel, A., Beals, M., Carothers, D., Chen, Y.-K., Conway, T., Gill, D., Grove, M., Hong, C.-Y., et al., "Electronic-photonic integrated circuits on the CMOS platform," in [*Silicon photonics*], **6125**, 612502, International Society for Optics and Photonics (2006).

[2] Miller, D. A., "Device requirements for optical interconnects to silicon chips," *Proceedings of the IEEE* **97**(7), 1166–1185 (2009).

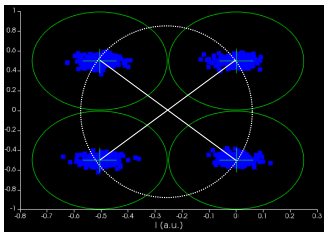

Figure 15. Constellations symbols diagram for the RAMZI modulator when used in QPSK modulation at 12.5 Gbaud (25 Gbps).

[3] Soref, R. and Bennett, B., "Electrooptical effects in silicon," *IEEE journal of quantum electronics* **23**(1), 123–129 (1987).

[4] Milivojevic, B., Wiese, S., Whiteaway, J., Raabe, C., Shastri, A., Webster, M., Metz, P., Sunder, S., Chattin, B., Anderson, S. P., et al., "Silicon high speed modulator for advanced modulation: device structures and exemplary modulator performance," in [*Silicon Photonics IX*], **8990**, 899013, International Society for Optics and Photonics (2014).

[5] Milivojevic, B., Wiese, S., Raabe, C., Shastri, A., Webster, M., Metz, P., Chattin, B., Dama, B., and Shastri, K., "Small-size silicon photonic iq modulator and low-power cmos driver for next generation coherent transceivers," in [*Proceedings of the 2013 18th European Conference on Network and Optical Communications & 2013 8th Conference on Optical Cabling and Infrastructure (NOC-OC&I)*], 181–184, IEEE (2013).

[6] Ziebell, M., Marris-Morini, D., Rasigade, G., Fédéli, J.-M., Crozat, P., Cassan, E., Bouville, D., and Vivien, L., "40 Gbit/s low-loss silicon optical modulator based on a pipin diode," *Optics express* **20**(10), 10591–10596 (2012).

[7] Jafari, O., Sepehrian, H., Shi, W., and LaRochelle, S., "High-Efficiency Silicon Photonic Modulator Using Coupled Bragg Grating Resonators," *Journal of Lightwave Technology* **37**(9), 2065–2075 (2019).

[8] Reed, G. T., Mashanovich, G., Gardes, F. Y., and Thomson, D., "Silicon optical modulators," *Nature photonics* **4**(8), 518 (2010).

[9] Witzens, J., "High-speed silicon photonics modulators," *Proceedings of the IEEE* **106**(12), 2158–2182 (2018).

[10] Samani, A., Chagnon, M., Patel, D., Veerasubramanian, V., Ghosh, S., Osman, M., Zhong, Q., and Plant, D. V., "A low-voltage 35-GHz silicon photonic modulator-enabled 112-Gb/s transmission system," *IEEE Photonics Journal* **7**(3), 1–13 (2015).

[11] Baehr-Jones, T., Ding, R., Liu, Y., Ayazi, A., Pinguet, T., Harris, N. C., Streshinsky, M., Lee, P., Zhang, Y., Lim, A. E.-J., et al., "Ultralow drive voltage silicon traveling-wave modulator," *Optics express* **20**(11), 12014–12020 (2012).

[12] Li, X., Yang, F., Zhong, F., Deng, Q., Michel, J., and Zhou, Z., "Single-drive high-speed lumped depletion-type modulators toward 10 fJ/bit energy consumption," *Photonics Research* **5**(2), 134–142 (2017).

[13] Gill, D., Green, W., Xiong, C., Rylyakov, A., Schow, C., Proesel, J., Rosenberg, J., Barwicz, T., Khater, M., Assefa, S., et al., "Distributed electrode mach-zehnder modulator with double-pass phase shifters and integrated inductors," *Optics express* **23**(13), 16857–16865 (2015).

[14] Zhang, Y., Yang, S., Lim, A. E.-J., Lo, G.-Q., Galland, C., Baehr-Jones, T., and Hochberg, M., "A compact and low loss y-junction for submicron silicon waveguide," *Optics express* **21**(1), 1310–1316 (2013).

[15] Lu, Z., Celo, D., Dumais, P., Bernier, E., and Chrostowski, L., "Comparison of photonic 2× 2 3-dB couplers for 220 nm silicon-on-insulator platforms," in [*2015 IEEE 12th International Conference on Group IV Photonics (GFP)*], 57–58, IEEE (2015).

[16] Bogaerts, W., De Heyn, P., Van Vaerenbergh, T., De Vos, K., Kumar Selvaraja, S., Claes, T., Dumon, P., Bienstman, P., Van Thourhout, D., and Baets, R., "Silicon microring resonators," *Laser & Photonics Reviews* **6**(1), 47–73 (2012).

[17] Almeida, V. R., Barrios, C. A., Panepucci, R. R., and Lipson, M., "All-optical control of light on a silicon chip," *Nature* **431**(7012), 1081 (2004).

[18] Sun, J., Sakib, M., Driscoll, J., Kumar, R., Jayatilleka, H., Chetrit, Y., and Rong, H., "A 128 Gb/s PAM4 silicon microring modulator," in [*2018 Optical Fiber Communications Conference and Exposition (OFC)*], 1–3, IEEE (2018).

[19] Biberman, A., Manipatruni, S., Ophir, N., Chen, L., Lipson, M., and Bergman, K., "First demonstration of long-haul transmission using silicon microring modulators," *Optics express* **18**(15), 15544–15552 (2010).

[20] Timurdogan, E., Sorace-Agaskar, C. M., Hosseini, E. S., and Watts, M. R., "An interior-ridge silicon microring modulator," *Journal of Lightwave Technology* **31**(24), 3907–3914 (2013).

[21] Gutierrez, A., Brimont, A., Rasigade, G., Ziebell, M., Marris-Morini, D., Fedeli, J.-M., Vivien, L., Marti, J., and Sanchis, P., "Ring-assisted Mach–Zehnder interferometer silicon modulator for enhanced performance," *Journal of Lightwave Technology* **30**(1), 9–14 (2011).

[22] Chang, C.-M., de Valicourt, G., Chandrasekhar, S., and Dong, P., "Differential microring modulators for intensity and phase modulation: Theory and experiments," *Journal of Lightwave Technology* **35**(15), 3116–3124 (2017).

[23] Jayatilleka, H., Murray, K., Guillén-Torres, M. Á., Caverley, M., Hu, R., Jaeger, N. A., Chrostowski, L., and Shekhar, S., "Wavelength tuning and stabilization of microring-based filters using silicon in-resonator photoconductive heaters," *Optics express* **23**(19), 25084–25097 (2015).

[24] Jayatilleka, H., Shoman, H., Chrostowski, L., and Shekhar, S., "Photoconductive heaters enable control of large-scale silicon photonic ring resonator circuits," *Optica* **6**(1), 84–91 (2019).

[25] Leinse, A., Diemeer, M., Rousseau, A., and Driessen, A., "A novel high-speed polymeric EO modulator based on a combination of a microring resonator and an MZI," *IEEE photonics technology letters* **17**(10), 2074–2076 (2005).

[26] Gill, D. M., Patel, S. S., Rasras, M., Tu, K.-Y., White, A. E., Chen, Y.-K., Pomerene, A., Carothers, D., Kamocsai, R. L., Hill, C. M., et al., "CMOS-compatible Si-ring-assisted Mach–Zehnder interferometer with internal bandwidth equalization," *IEEE Journal of Selected Topics in Quantum Electronics* **16**(1), 45–52 (2009).

[27] Akiyama, S., Kurahashi, T., Morito, K., Yamamoto, T., Usuki, T., and Nomura, S., "Cascaded-ring-resonator-loaded Mach–Zehnder modulator for enhanced modulation efficiency in wide optical bandwidth," *Optics Express* **20**(15), 16321–16338 (2012).

[28] Romero-García, S., Moscoso-Mártir, A., Azadeh, S. S., Müller, J., Shen, B., Merget, F., and Witzens, J., "High-speed resonantly enhanced silicon photonics modulator with a large operating temperature range," *Optics letters* **42**(1), 81–84 (2017).

[29] Guha, B., Kyotoku, B. B., and Lipson, M., "CMOS-compatible athermal silicon microring resonators," *Optics express* **18**(4), 3487–3493 (2010).

[30] "CWDM8 MSA Group Releases 400G 10 km Optical Interface Specification for Data Center Optical Links." https://www.businesswire.com/news/home/20171220005292/en/CWDM8-MSA-Group-Releases-400G-10-km (2017).

[31] "[press release] industry leaders form open eye msa consortium, and optomind named founding member." http://optomindinc.com/press-release-industry-leaders-form-open-eye-msa-consortium-and-optomind-name?ckattempt=1 (2019).

[32] "IEEE 802.3bs-2017 - IEEE Standard for Ethernet Amendment 10: Media Access Control Parameters, Physical Layers, and Management Parameters for 200 Gb/s and 400 Gb/s Operation." https://standards.ieee.org/standard/802_3bs-2017.html (2018).

[33] Li, R., Patel, D., Samani, A., El-Fiky, E., Xing, Z., Morsy-Osman, M., and Plant, D. V., "Silicon photonic ring-assisted mzi for 50 gb/s dac-less and dsp-free pam-4 transmission," *IEEE Photonics Technology Letters* **29**(12), 1046–1049 (2017).

[34] Shi, W., Xu, Y., Sepehrian, H., LaRochelle, S., and Rusch, L. A., "Silicon photonic modulators for PAM transmissions," *Journal of Optics* **20**(8), 083002 (2018).

[35] Samani, A., El-Fiky, E., Osman, M., Patel, D., Li, R., Jacques, M., and Plant, D., "180 gb/s single carrier single polarization 16-qam transmission using an o-band silicon photonic iqm," *Optics express* **27**(10), 14447–14456 (2019).

[36] Chaichuay, C., Yupapin, P. P., and Saeung, P., "The serially coupled multiple ring resonator filters and Vernier effect.," *Optica Applicata* **39**(1) (2009).

[37] Fu, Y., Zhang, X., Hraimel, B., Liu, T., and Shen, D., "Mach-zehnder: a review of bias control techniques for mach-zehnder modulators in photonic analog links," *IEEE microwave magazine* **14**(7), 102–107 (2013).

[38] Harris, N. C., Ma, Y., Mower, J., Baehr-Jones, T., Englund, D., Hochberg, M., and Galland, C., "Efficient, compact and low loss thermo-optic phase shifter in silicon," *Optics express* **22**(9), 10487–10493 (2014).

[39] Streshinsky, M., Ding, R., Liu, Y., Novack, A., Yang, Y., Ma, Y., Tu, X., Chee, E. K. S., Lim, A. E.-J., Lo, P. G.-Q., et al., "Low power 50 Gb/s silicon traveling wave Mach-Zehnder modulator near 1300 nm," *Optics express* **21**(25), 30350–30357 (2013).

[40] Li, Z.-Y., Xu, D.-X., McKinnon, W. R., Janz, S., Schmid, J. H., Cheben, P., and Yu, J.-Z., "Silicon waveguide modulator based on carrier depletion in periodically interleaved pn junctions," *Optics express* **17**(18), 15947–15958 (2009).

[41] Rosenberg, J., Green, W., Assefa, S., Gill, D., Barwicz, T., Yang, M., Shank, S., and Vlasov, Y. A., "A 25 gbps silicon microring modulator based on an interleaved junction," *Optics express* **20**(24), 26411–26423 (2012).

[42] Zhang, L., Li, Y., Yang, J.-Y., Song, M., Beausoleil, R. G., and Willner, A. E., "Silicon-based microring resonator modulators for intensity modulation," *IEEE Journal of Selected Topics in Quantum Electronics* **16**(1), 149–158 (2009).